Beam conditioning for electron energy recovery systems in devices employing axis-encircling beams

A. SINGH†, W. LAWSON†, D. GOUTOS†, W. R. HIX†,
C. D. STRIFFLER†, V. L. GRANATSTEIN†
and W. W. DESTLER†

Depressed collectors are extensively used in linear-beam devices. In spiralling beam devices, the motion of the spent beam needs to be converted into axial motion before it can deliver energy to the retarding axial electrostatic field produced by depressed collectors. A method of doing so is presented here, along with simulation results. A large-orbit gyrotron is chosen as an illustrative example in which the axis-encircling beam is generated by passing an axially streaming beam through a magnetic cusp. After rf interaction, an 'unwinding' of the beam is done by a second magnetic cusp with a reversed magnetic field. The trajectories of electrons going through the two cusps have been simulated in order to evaluate the effects of finite cusp width and finite width of emitting surface. Also studied are the effects of variations of the magnetic field, the accelerating voltage of the beam, and the distance between cusps. These simulations show that the rotational energy of electrons is largely converted into axial energy after passage through the second cusp. An initial geometry has been chosen for three collectors, of which two are at depressed potentials. Changes in the energies of the particles are introduced between the two cusps as an approximation of the effect of rf interaction. Simulation of trajectories in the region of the depressed collectors has demonstrated energy sorting of the beamlets to different depressed collectors.

1. Introduction

Gyrotron oscillators operating at the fundamental cyclotron frequency have made great strides in achieving high rf power levels at high frequencies with appreciable efficiencies of operation (Granatstein 1984, 1987, Fix *et al.* 1984, Rager 1986). Other device configurations using spiralling electron beams have unfortunately suffered from significantly lower electronic efficiencies.

Among such devices are those that use axis-encircling beams. These include large-orbit gyrotrons (Lawson *et al.* 1985) and circular geometry free-electron lasers (Befeki *et al.* 1985). Those of the former category of devices, in which the axis-encircling beam is generated by a magnetic cusp, have been referred to as cusptrons (Uhm *et al.* 1984). Those in which the electromagnetic field is supported by a magnetron-like structure have also been called gyromagnetrons (Lau and Barnett 1982, Grow and Shrivastava 1982). The nature of the beam and the rf structure favours the production of coherent radiation at a chosen high harmonic of the cyclotron frequency. As the value of the magnetic field required for any given frequency is reduced in the ratio of the harmonic number, this would be a significant advantage for operation at millimetre wavelengths (Chojnacki *et al.* 1987). However, efficiency usually falls as the harmonic number rises, and this implies that a con-

† Laboratory for Plasma and Fusion Energy Studies, University of Maryland, College Park, MD 20742-3511, USA.

siderable proportion of the initial kinetic energy of the beam would be carried by the spent beam.

One possibility for improving the overall efficiency of such devices is to recover energy from the spent beam. In the case of linear beam tubes, such as travelling wave tubes, this is a well-accepted approach (Kosmahl 1982, True 1987). The spent beam is sorted into groups energy-wise, and is collected on electrodes at depressed potentials. The geometry and the potentials of the collectors are chosen to make for as soft a landing as possible for each group. Thus, a good fraction of the energy of the beam is transferred back to the power supply system. This has the additional advantage of reducing the bulk and cost of the power supply.

The overall efficiency of the device η_T is related to the intrinsic efficiency η_e and the efficiency of energy recovery η_R by the relationship (Arnush *et al.* 1982)

$$\eta_T = \frac{\eta_e}{1 - \eta_R(1 - \eta_e)}. \tag{1}$$

Thus, if a device of 10% intrinsic efficiency is operated in tandem with depressed collectors at 75% efficiency, the overall efficiency would be 31%.

In the case of devices where the spent beam has most of its energy in rotational motion, the electrons cannot work effectively against the electrostatic field of the depressed collectors. Thus, it is necessary to convert the rotational motion largely into axial motion before leading the beam toward depressed collectors. In linear-beam tubes, transverse motion in the spent beam arising out of the effects of the focusing magnetic field and rf interaction is partially converted into axial motion by an adiabatic expansion of the beam (Kosmahl 1982). In the case of axis-encircling beams, the Larmor radius of the beam electrons is usually large, and would be further increased by adiabatic expansion before the process of energy sorting starts. The latter process itself involves further radial expansion and an increase of the aperture of each of successive depressed collectors. Thus, adiabatic expansion, apart from requiring a slow change of magnetic field over a distance, involves considerable enlargement of the dimensions of axis-encircling beam devices.

We have proposed 'unwinding' the beam by passing it through a second cusp with a reversed magnetic field. Its radial magnetic field component acts on the azimuthal component of velocity and converts it largely into axial velocity; this is a non-adiabatic process. As shown by these studies, a substantial fraction of the energy in the rotational motion of the electrons is reconverted into axial motion in a distance that is small compared with the pitch of the spiralling motion and with little change in the diameter of a hollow beam.

The extent of this reconversion is dependent upon various parameters. We have studied the reconversion phenomenon as a function of the transition widths of two cusps, the distance been them, the radial width of the beam, the magnetic field amplitude, and the accelerating voltage of the beam. A single particle code was used to plot the trajectories. The results of these simulations are presented here. They verify the applicability of the basic approach in that the fraction of energy converted into axial motion is close to 90% even with a non-optimum combination of parameters.

We have also simulated the trajectories of particles with different energies in the region of the depressed collectors. For this purpose a system of three collectors, two of which are at depressed potentials, is chosen as an initial example. Energy sorting under the combined action of the magnetic and electrostatic fields is demonstrated.

In §2, the results of computer simulations relating to the unwinding of a spiralling, large-orbit beam by a second cusp under various conditions are reported. Section 3 presents the trajectories in the collector region and verifies energy sorting. Section 4 outlines the design considerations in the planned experiment, and conclusions are drawn in §5.

2. Generation and unwinding of spiralling electron beams

An axis-encircling beam for a large orbit gyrotron can be generated by passing an axially streaming beam through a magnetic cusp, which has a sharp reversal of magnetic field (Rhee and Destler 1974). The behaviour of an electron beam passing through such a cusp has been studied in the cases of an ideal cusp as well as a cusp with a finite transition width (Scheitrum and True 1981, Rhee and Destler 1974). The cases studied include a balanced cusp, which implies an exact reversal of the field on the two sides of the cusp, as well as more generalized changes of field across the cusp (Destler and Rhee 1977).

A solution of the equations of motion shows that for a spiralling electron passing through an ideal cusp, the guiding centre radius upstream equals the Larmor radius downstream (Rhee and Destler 1974). As a special case we note that an electron travelling axially at a radius r_0 through an ideal and balanced cusp acquires a spiralling motion, whose guiding centre lies on the axis and whose Larmor radius equals r_0. An annular sheet beam of radius r_0 correspondingly emerges as a uniform rotating cylinder. Considering the case of two ideal cusps separated by a certain distance, the electron would have a zero Larmor radius beyond the second cusp and a guiding centre radius of r_0, i.e., an axially-streaming beam.

A schematic diagram of a configuration which is the subject of study here is shown in Fig. 1. A stream of electrons starts from a ring cathode and is formed by a Pierce gun into an axially-streaming annular beam. After passing the first cusp, the beam passes through a region which has an rf structure. The beam then goes through the second cusp (that has a reversed field), which tends to unwind the spiralling motion before the beam proceeds toward the depressed collectors.

In practice, the transition region in the cusps has a finite width. An approximation to the field variation across the cusp which has been used with success is as follows (Destler *et al.* 1988, Lawson and Latham 1987):

$$B_z(r_0, z) = B_0 \tanh \frac{z}{\zeta} \tag{2}$$

where B_0 is the asymptotic magnitude of the axial magnetic field on the two sides of a balanced cusp, and ζ is a parameter that is the measure of the transition width along the z-axis. In this case, the guiding centre downstream of the cusp no longer lies on the axis. Considering all electrons in a thin hollow beam starting at a given radius, the finite cusp width gives rise to a scalloping of the post cusp beam envelope. The scalloping wavelength to zeroth-order is given by

$$\lambda = 2\pi r_0(\eta^2 - 1)^{1/2} \tag{3}$$

which is the electron axial pitch distance for an ideal cusp; and where $\eta \triangleq v_{z_1}/r_0\Omega$; v_{z_1} is the axial velocity upstream of the cusp, $\Omega = eB_0/m\gamma$ is the relativistic cyclotron frequency, and γ is the relativistic mass factor.

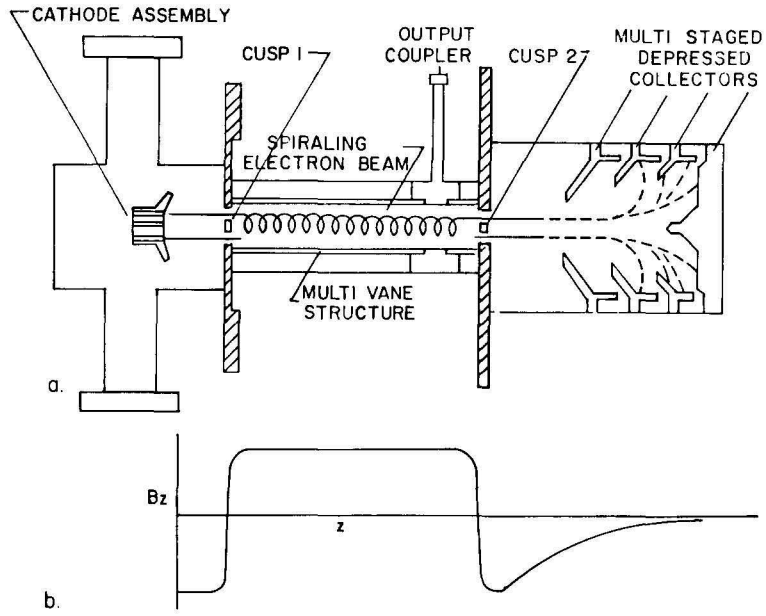

Figure 1. Schematic diagram of a configuration which is the subject of study here. A stream of electrons starts from a ring cathode and is formed by a Pierce gun into an axially-streaming annular beam. After passing the first cusp, which causes the beam to spiral, the beam passes through a region which has an rf structure. The beam then goes through the second cusp (that has a reversed field), which tends to unwind the spiralling motion before the beam proceeds towards the depressed collectors.

For this study, a parameter which acts as a useful index of the effects of the two cusps is α, defined as the ratio of the transverse to the axial component of velocity, i.e.,

$$\alpha \triangleq \frac{v_\perp}{v_\parallel} \tag{4}$$

In order to obtain some figures for a typical set of operating parameters and to gain a better insight into their interrelationships, trajectories were simulated under different conditions. A single particle code was used for tracing the path of the electrons through the cusped magnetic fields. The code numerically integrates particle orbits through the cusp fields. The code uses, as a model for the cusp, the axial component of the magnetic field as given in eqn. (2). A gaussian profile is used for the radial component of the field and a Taylor expansion of the fields about $r = r_0$ is performed. See Destler *et al.* (1988) and Lawson and Latham (1987) for more details on the code. The initial values of the static parameters were close to the experimental values for the low energy cusptron operated earlier at the University of Maryland. These were: $B_0 = 328{\cdot}8$ gauss, $r_0 = 1{\cdot}5\,\text{cm}$, accelerating voltage $V_0 = 26\,\text{kV}$, and $\zeta = 4\,\text{mm}$.

From such a simulation, an illustrative example of the variation of α with the axial position is shown in Fig. 2. The value of α goes from zero upstream of the cusp to a finite value in the region between the cusps, denoted by α_{midrange}. It falls to a low value as the beam passes through the second cusp, denoted by α_{residual}. As the

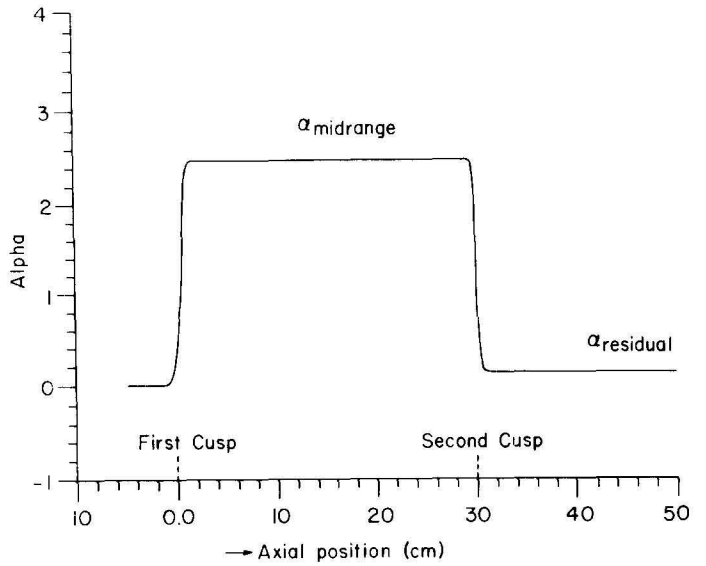

Figure 2. Illustrative example of the variation of $\alpha = v_\perp/v_\parallel$ along the axial coordinate. It rises from zero to a value called α_{midrange} as the electrons pass the first cusp, located at 0 cm, and falls again to a low value called α_{residual} after the electrons pass the second cusp, located at 30 cm: $B_0 = 340$ gauss, $r_{\text{start}} = 1{\cdot}5$ cm, $\zeta_{1,2} = 4$ mm, and $V_0 = 26$ kV.

cusps have a finite width, the value of α_{residual} turns out to be finite rather than zero as in the ideal cusp limit.

Various geometric and electrical parameters influence the trajectories, α_{midrange} as well as α_{residual}. These were studied by varying the parameters one by one. The results are reported in the following subsections.

2.1. *Variation of* α *with* B_0

For the case of the ideal cusp where the transverse velocity component is purely azimuthal, the value of α_{midrange} is given by:

$$\alpha_{\text{midrange}} = \frac{r_0 \Omega}{[v_{z_1}^2 - (r_0 \Omega)^2]^{1/2}} \tag{5}$$

The results of particle code simulations performed to determine the effect of variations of B_0 are summarized in Fig. 3(*a*). As seen from eqn. (5), α_{midrange} is a monotonically rising function of B_0. It is also seen that α_{residual} goes through a cyclic variation. This variation is associated with the radial scalloping of the electrons between the two cusps and the resulting variation in particle angle as it enters the second cusp. The physical explanation of this and cyclic variations with other parameters are discussed in §2.6. Here it may be noted that as B_0 increases, the cyclic variation occurs at shorter intervals, due to a progressive decrease in the scalloping wavelength.

As a general trend, the value of α_{residual} is less than α_{midrange} by a factor of ten or more. The maximum value of α_{residual} is mostly below 0·3. Consequently, the energy in rotational motion is less than 10% of the energy in axial motion.

For most of the other simulation runs, the distance between the two cusps, z_{c_2},

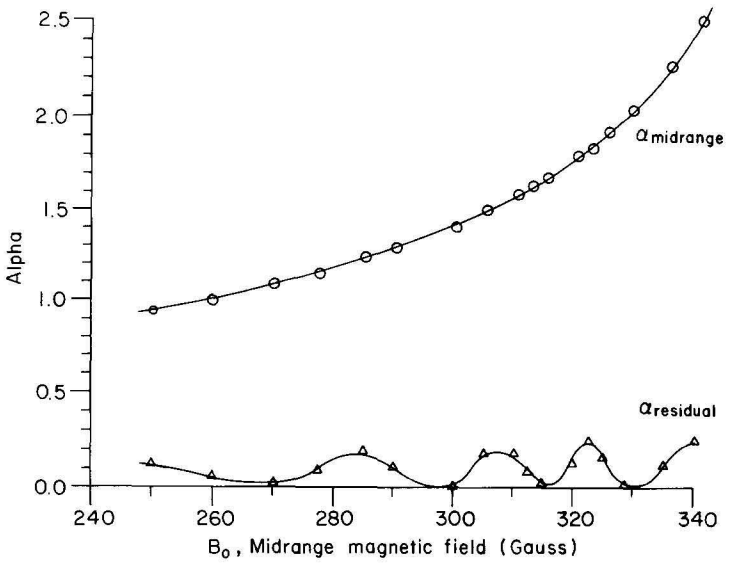
2.5
2.0
1.5
1.0
0.5
0.0
Alpha
$\alpha_{midrange}$
$\alpha_{residual}$
240
260
280
300
320
340
B_0, Midrange magnetic field (Gauss)

(*a*)

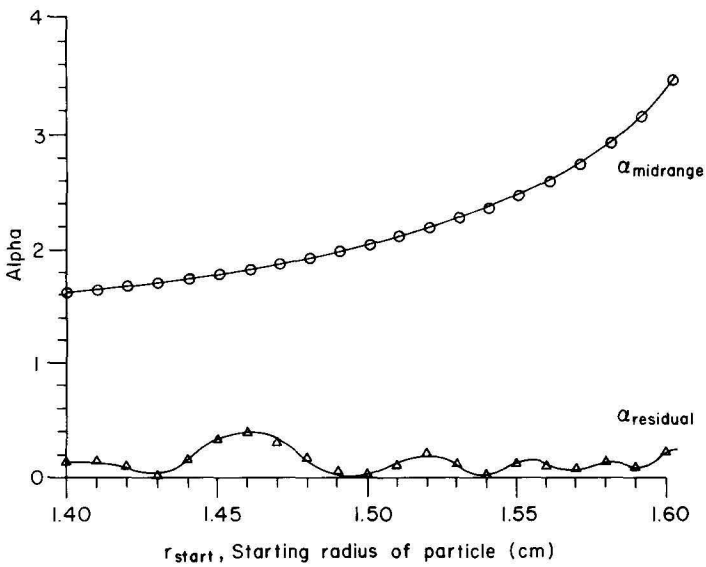
4
3
2
1
0
Alpha
$\alpha_{midrange}$
$\alpha_{residual}$
1.40
1.45
1.50
1.55
1.60
r_{start}, Starting radius of particle (cm)

(*b*)

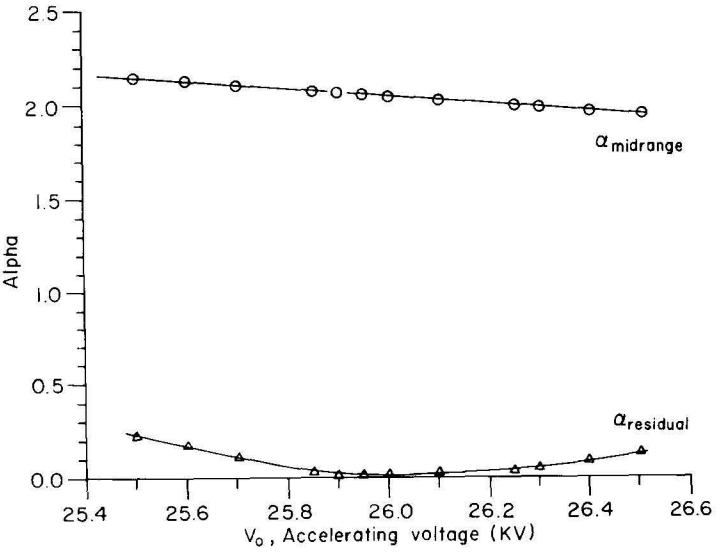

(*c*)

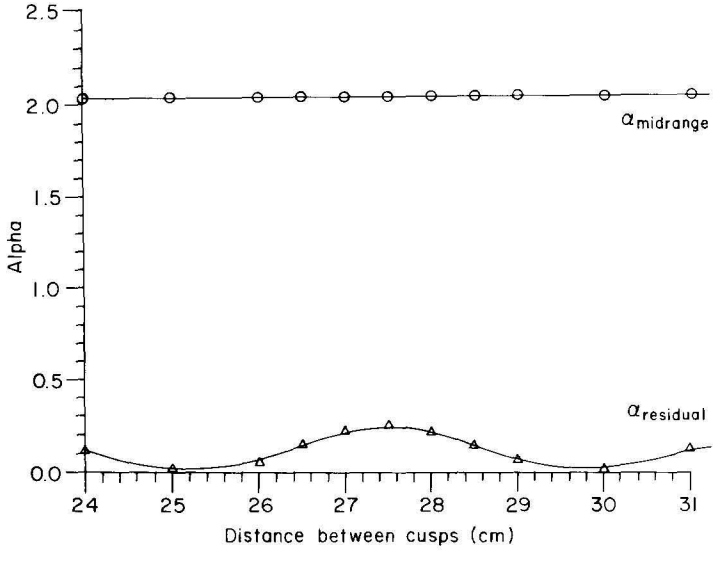

(*d*)

Figure 3. Results of particle code simulations relating to the effect of variations in different parameters on $\alpha_{midrange}$ and $\alpha_{residual}$. Median values of the parameters are: $V_0 = 26\,kV$, second cusp at 30 cm, $r_{start} = 1{\cdot}5\,cm$, $\zeta_{1,2} = 4\,mm$, and $B_0 = 328{\cdot}8$ gauss. (*a*) Effect of variation of B_0; (*b*) effect of variation of r_{start}, the starting radius of the particle; (*c*) effect of variation of V_0, the accelerating voltage; and (*d*) effect of variation of distance between cusps.

was chosen as 30 cm. For this value of separation and $B_0 = 328{\cdot}8$ gauss, the value of $\alpha_{residual}$ was 0·014. Clearly, this is the optimum position to produce low transverse energy, and thus increased depressed collector efficiency. This is subject to a narrow range of variation of the starting radius, as discussed in the next section.

2.2. *Variation of α's with starting position of electrons*

For a given value of B_0, the radius at which the electron starts, denoted by r_{start}, influences $v_\perp$, $v_\parallel$, and α. For an annular cathode with finite width, the value of $\alpha_{midrange}$ would thus depend upon the starting position of the electron (substitution of r_{start} for r_0 in eqn. (5)). For this reason, it is advisable to limit the percentage of variation in r_{start} to a small value. Also, the choice of value of B_0 should not be too close to the threshold value of the magnetic field for which the particles reflect (Rhee and Destler 1974), for otherwise the variations in α due to the variation in r_{start} will be too large.

Figure 3(*b*) shows the variations of $\alpha_{midrange}$ and $\alpha_{residual}$ with the starting positions of the particle. As expected, $\alpha_{midrange}$ rises monotonically with r_{start}. Furthermore, the value of $\alpha_{residual}$ varies cyclically with r_{start}. Recall that as $\alpha_{midrange}$ changes, the number of gyrations completed between the two cusps changes. Because of the finite width of the cusps, the beam would have a scalloping motion whose phase of arrival at the second cusp would depend upon r_{start}, resulting in the cyclic variation of $\alpha_{residual}$.

The highest value of $\alpha_{residual}$, corresponding to $r_{start} = 1{\cdot}46$ cm, is 0·37. For the range of values of r_{start} for the actual cathode, from 1·4–1·6 cm, the $\alpha_{residual}$ lies for the most part between 0·01 and 0·2, indicating a good percentage of energy conversion from rotational to axial motion. It is observed that if the distance between the cusps is changed, the value of r_{start} for the maximum value of $\alpha_{residual}$ is also altered.

2.3. *Variations of α's with accelerating voltage*

Trajectory simulations were done for a narrow range of accelerating voltages, V_0, from 25·5–26·5 kV. As seen in Fig. 3(*c*), $\alpha_{midrange}$ decreases slowly from 2·15 to 1·94, while $\alpha_{residual}$ rises from 0·005 at the median value of V_0 to 0·225 and 0·122 at the two extremes. These changes are due to variation from optimum in the phase of scalloping at the second cusp.

2.4. *Variation of $\alpha_{residual}$ with distance between the cusps*

As expected, the $\alpha_{midrange}$ is dependent upon the electrical parameters and those of the first cusp only. Figure 3(*d*) shows the variation of $\alpha_{residual}$ with the location of the second cusp with respect to the first one. It is seen that the variation is cyclic between the values 0·014 and 0·250. These values are satisfactory from the point of view of energy conversion. The cyclic nature of the variation is discussed in section 2.6.

2.5. *Variation of $\alpha_{residual}$ with transition width of the cusps*

As the cusp half-width, ζ, was varied from 2·0–5·0 mm for both cusps, the $\alpha_{midrange}$ simultaneously increased slowly from 2·02–2·06, and the $\alpha_{residual}$ decreased

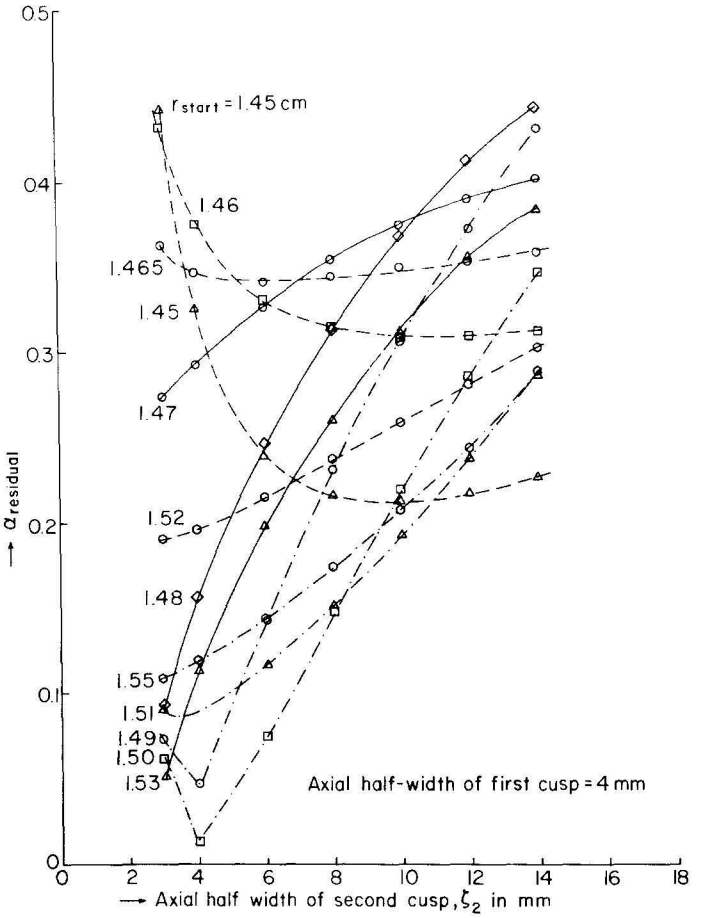

Figure 4. Plots showing variations of $\alpha_{residual}$ with ζ_2 the half-width of the second cusp going from 3–14 mm. The parameter ζ_1, the half-width of the first cusp, equals 4 mm.

slowly from 0·029–0·006. Thus, although an increase in the cusp width increases the shift of the guiding centre from the axis, thus increasing the scalloping; the changes in α are small. The values of $v_\perp$ and $v_\parallel$ depend essentially on B_0. The trajectories, however, are influenced by the modelling of the field in the transition region. The model tends to be less accurate as one moves away from the median value of r_{start} and near to the corners of the iron cusp material.

Furthermore, the value of $\alpha_{residual}$ was determined for $r_{start} = 1{\cdot}46$ cm (the worst case defined in §2.2), as well as for other values of r_{start} for a variation of ζ of the second cusp from 3–14 mm, keeping ζ for the first cusp equal to 4 mm, as shown in Fig. 4.

It is seen that for starting radii such as 1·45 cm, which give a relatively high $\alpha_{residual}$ at $\zeta_2 = 3$ mm, the $\alpha_{residual}$ diminishes as ζ_2 increases and goes through a broad minimum near $\zeta_2 = 10$ mm. For starting radii such as 1·50 cm, which gives a very low value of $\alpha_{residual}$ for $\zeta_2 = 3$ mm, the $\alpha_{residual}$ has a sharp minimum at $\zeta_2 =$ 4 mm and progressively rises as ζ_2 increases further to 14 mm.

The maximum swing in $\alpha_{residual}$ with variation in r_{start} is by a factor of nearly 40,

when both ζ_1 and ζ_2 are 4 mm. However, this factor is only two when ζ_2 has risen to 14 mm. Broadly speaking, this phenomenon can be understood as follows. Changes in $\alpha_{residual}$ occur due to variations in r_{start}, because the latter changes the phase of scalloping in which the particle enters the second cusp. If the second cusp is narrow, the phase relationship is sharply defined, resulting in clear-cut reinforcement or cancellation of the radial component of velocity due to the two cusps. When the two cusps are narrow and of equal width, the cancellation can be nearly complete, at a favourable phase relationship. However, when the second cusp is broad, there is a correspondingly large change in the phase of scalloping during transit through the cusp. Consequently, reinforcement or cancellation is not very sharply defined. The general trend is for $\alpha_{residual}$ to increase as ζ_2 rises.

2.6. *Cause of cyclic variations in* $\alpha_{residual}$

The solution of the equations of motion shows that for the case of a finite transition width of a cusp, the charged particle acquires a positive radial component of velocity as it passes through the cusp. This, in fact, causes a shift in the positions of the guiding centre away from the axis and results in scalloping.

When the particle approaches the second cusp, its scalloping motion may have given it a positive or negative component of radial velocity, depending on its phase in the scalloping cycle. If the particle is moving outward as it approaches the second cusp, the radial motion is accentuated, thus giving rise to a relatively larger value of $\alpha_{residual}$. The reverse is true for the case of the particle approaching the second cusp with an inward motion, which then wholly or partly is compensated for by the effect of the second cusp.

In this connection, it is relevant to look at the trajectories of the particles from an end on position. Figure 5 shows such a projection in the x-y plane for two

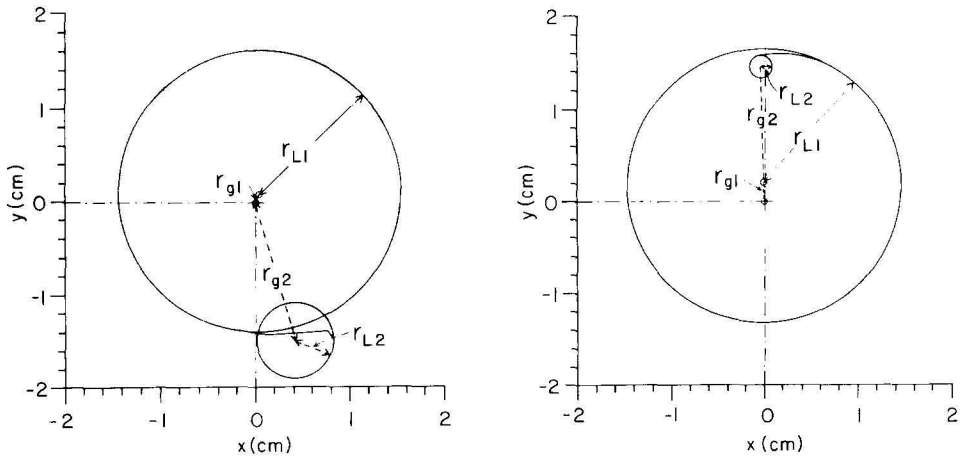

Figure 5. Trajectories of the particles as seen from an end-on position showing a projection in the transverse (x-y) plane for two particles. In each case, the larger circle represents an end-on view of the spiralling motion in the midrange region (subscript 1), and the smaller circle represents the residual spiralling motion beyond the second cusp (subscript 2). In (*a*) the particle is going outward as it goes through the second cusp, and the circle showing residual motion is larger than the case (*b*) where the particle is going inward as it enters the second cusp.

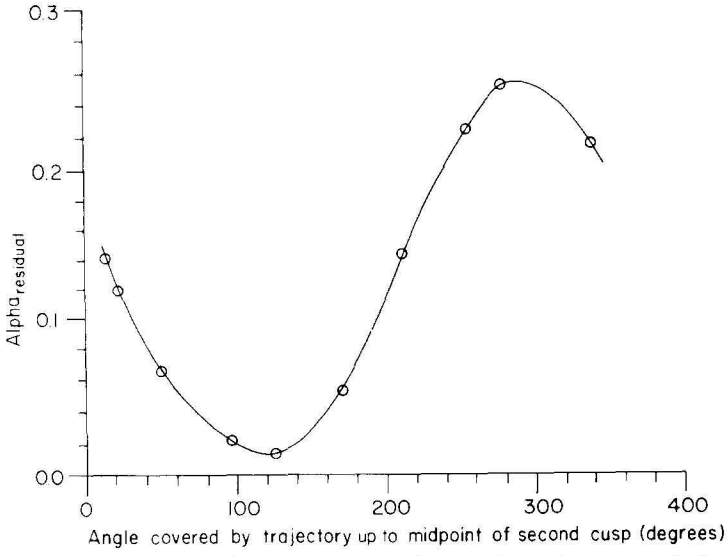

Figure 6. Plots of the value of the $\alpha_{residual}$ versus the transit angle, over and above complete cycles for the case where the change in the transit angle is due to the change in location of the second cusp. The points represent snapshots which do not all belong to one and the same cycle. $V_0 = 26\,kV$, second cusp at 30 cm, $r_{start} = 1{\cdot}5\,cm$, $\zeta_{1,2} = 4\,mm$, and $B_0 = 328{\cdot}8$ gauss.

particles. In each case, the larger circle represents an end-on view of the spiralling motion in the midrange region with a larger Larmor radius. The smaller circle represents the residual spiralling motion beyond the second cusp, which has a smaller Larmor radius. This second circle is seen to have a larger diameter in Fig. 5(*a*) when the particle is moving outward from the larger to the smaller circle than in Fig. 5(*b*), where the trace connecting the two is moving inward. The off-axis locations of the guiding centre are clearly seen.

The value of $\alpha_{residual}$ versus the transit angle (modulo 2π) was plotted for the case when the change in the transit angle is due to the change in location of the second cusp and is shown in Fig. 6. The one cycle shown is, in fact, a synthesis of snapshots of points occurring over more than one cycle seen in Fig. 3(*d*). A similar curve was obtained when the change in transit angle was due to a change in the magnetic field, B_0, while keeping the distance between the cusps constant. This corroborates the physical explanation of the cause of the cyclic variations discussed above.

Correlation between transit angle and $\alpha_{residual}$ was also seen to be good in the case of variations due to a change in ζ. However, the scatter of points was larger in the case of variations caused by changes in r_{start}. This is attributed to the fact that when r_{start} is changed, it changes not only the $\alpha_{midrange}$ and the scalloping wavelengths but also shifts the trajectories farther away from the median radius of the hollow beam. In that case, the field profiles and the effective cusp width vary. The $\alpha_{residual}$ changes cyclically with transit angle but not on an equally smooth curve.

2.7. *Variation in the range of scalloping*

The range of scalloping, as defined by the difference between the maximum and minimum radii of the trajectories, was studied in the region between the cusps and

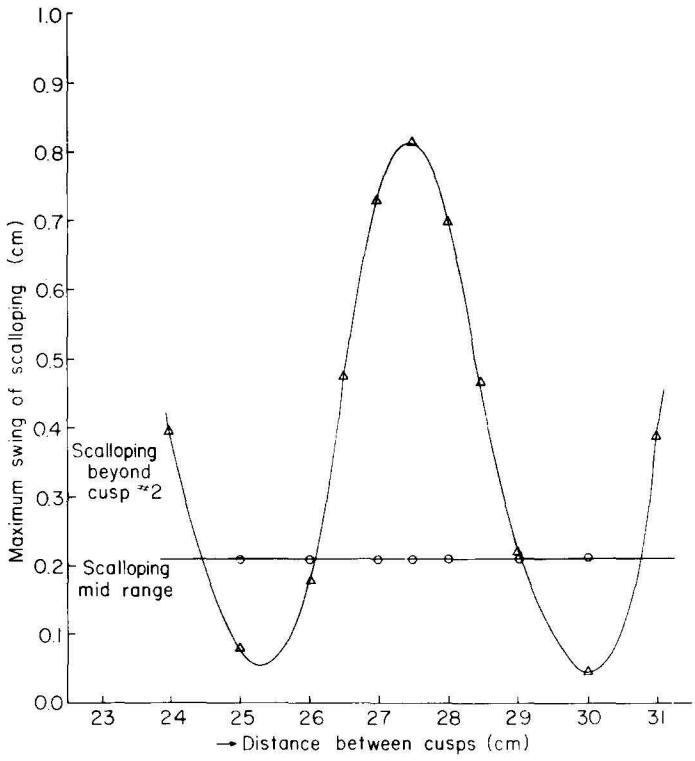

Figure 7. The range of scalloping, as defined by the difference between the maximum and minimum radii of the trajectories in the region between the cusps and beyond the second cusp. Shown is the case of variations due to distance between cusps, $B_0 =$ 328·8 gauss, $r_{start} = 1{\cdot}5$ cm, $V_0 = 26$ kV, and $\zeta_{1,2} = 4$ mm.

beyond the second cusp. Figure 7 shows the case of variations in the range scalloping due to variation in the distance between the cusps. The cyclic variations in scalloping beyond the second cusp are seen to resemble the variations in $\alpha_{residual}$. The scalloping in the midrange region is, of course, dependent only on the parameters of the first cusp, and is therefore not a function of the distance between cusps.

2.8. *Correlation between analytical and numerical results*

The parameters $\lambda_{scalloping}$ and $\alpha_{midrange}$ can be evaluated both from numerical simulations and the analytical relationships given in eqns. (3) and (5). The results for $\alpha_{midrange}$ are shown in Figs. 8(*a*) and (*b*) and agree very closely. When the independent variable is B_0, the difference is 0·4% for $B_0 = 260$ gauss and 1% for $B_0 = 340$ gauss, with the respective values of α being 1·0 and 2·5. Where the independent variable is r_{start}, the difference is 0·4% for the median value of r_{start} and rises to 6% for $r_{start} = 1{\cdot}4$ and 1·6 cm. Plots of the numerical and analytical values of $\lambda_{scallop}$ as a function of the starting radius are shown in Fig. 9. The difference varies from 2% near the median value of r_{start} to 6% at $r_{start} = 1{\cdot}6$ cm. These differences are due to a combination of finite mean cusp width and variation of cusp width about the mean value.

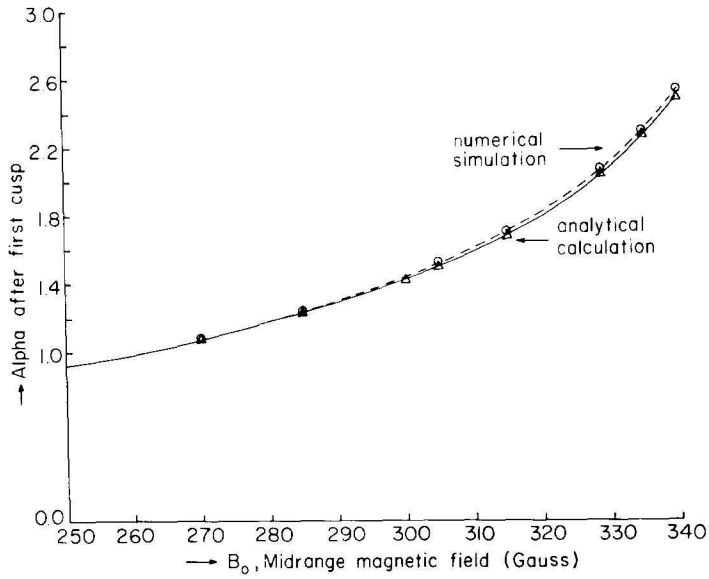

(*a*)

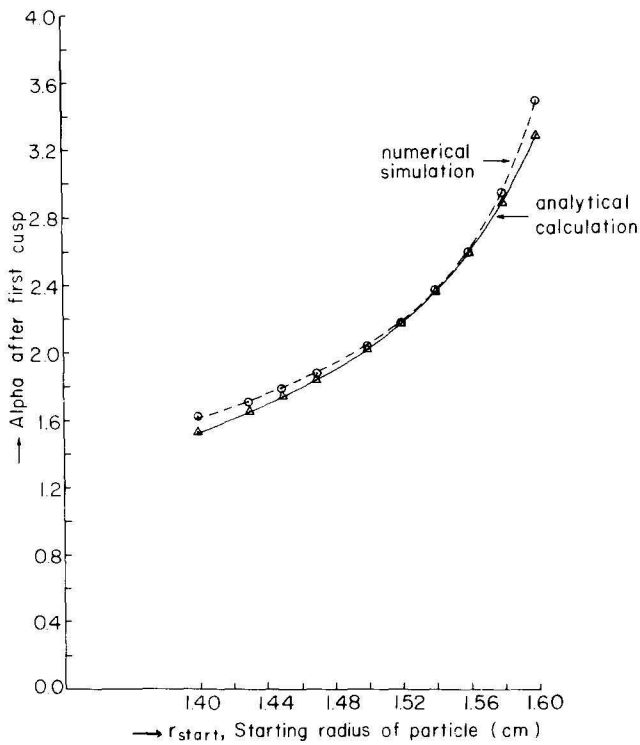

(*b*)

Figure 8. A comparison of values of α_{midrange} obtained from analytical and numerical techniques. (*a*) Variation of α with B_0. The difference is 0·4% at $B_0 = 260$ gauss and 1% at $B_0 = 340$ gauss; $V_0 = 26\,\text{kV}$, $r_{\text{start}} = 1{\cdot}5\,\text{cm}$, and $\zeta_1 = 4\,\text{mm}$. (*b*) Variation of α with r_{start}. The difference is 0·4% at $r_{\text{start}} = 1{\cdot}52\,\text{cm}$ and 6% at 1·40 and 1·60 cm: $B_0 = 328{\cdot}8$ gauss, $\zeta_{1,2} = 4\,\text{mm}$, and $V_0 = 26\,\text{kV}$.

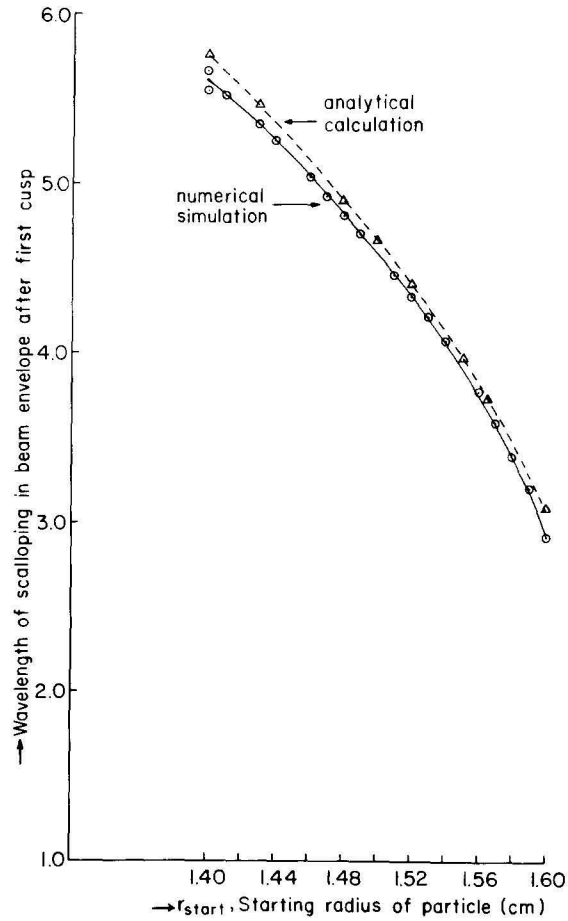

Figure 9. A comparison of the values of scalloping wavelength versus starting radius of the particle as obtained from analytical and numerical techniques. The difference varies between 2% and 6%. $B_0 = 328{\cdot}8$ gauss, $V_0 = 26$ kV, and $\zeta_1 = 4$ mm.

3. Energy sorting in the collector region

With its rotational motion converted sufficiently into axial motion, the beam would be ready to enter the region of depressed collectors. The geometry and the potentials in the collectors, as well as the magnetic field profile, have to be suitably chosen. The objective is that the combined effect of this electrostatic field and the magnetic field cause the trajectories of electrons of different energy ranges to be sorted out to different electrodes with depressed potentials as close to the energy of that group as possible. The larger the energy spread due to rf interaction and the more ambitious the target value for collector efficiency, the larger the number of depressed collectors that would be required.

In the present case, considering the fact that a large-orbit gyrotron operating in a high harmonic mode has a low efficiency, a configuration was chosen consisting of three collectors, two of which are at depressed potentials. In choosing the geometry, a consideration kept in mind is that a small component of radial electric field is

introduced in the collector region which opposes the motion of any secondary electrons emitted at the collector surfaces back toward the axis.

The Herrmannsfeldt code (Herrmannsfeldt 1979) has been used for calculating the trajectories of the particles. The magnetic field profile is also evaluated by specifying the position, the geometry, and the current through each ideal N-turn coil. The effect of the iron plate that generates the second cusp was simulated by an image of the coil nearest to the iron plate.

The potentials on the depressed collectors, as well as the parameters of the coils, were adjusted for suitable energy sorting. The electrode potentials were set at 0, $-12{\cdot}5$, and -20 kV. The magnetic field was always adjusted to make it a balanced cusp.

In fixing the parameters for trajectory studies, the energy of the electron beam entering the first cusp was initially assumed to be 26 keV, corresponding to an earlier experiment on cusptron operation at the University of Maryland (Chojnacki *et al.* 1987). In order to simulate the conversion of a part of the energy in the beam into rf in the region between the cusps, the particles were divided into five groups. Energy changes were introduced to correspond to -30%, -20%, -10%, 0%, and $+10\%$ of 26 keV. The radial location at which the particles emerged from the second cusp, as well as their angles, were noted from single particle trajectory code simulation. These were then used as inputs to the Herrmannsfeldt code simulation of trajectories in the collector region. The trajectories are shown in Fig. 10. The beam current was assumed to be one ampere, as in the earlier experiment.

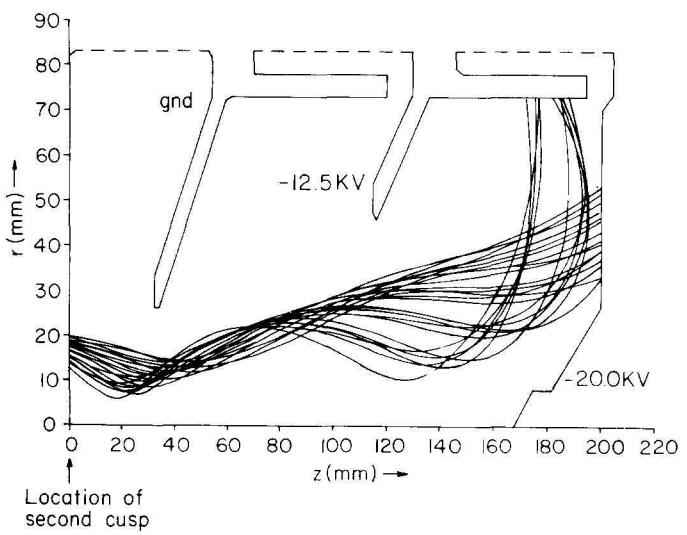

Figure 10. Electron trajectories in the collector region for electrodes at ground, $-12{\cdot}5$ kV, and -20 kV. The beamlets of energies 18·2 and 20·8 keV are collected at $-12{\cdot}5$ kV; those of energies 23·4, 26·0, and 28·6 keV are collected at -20 kV.

It is seen that the beamlets of energies 18·2 and 20·8 keV are collected at the electrode at −12·5 kV, and those of energies 23·4, 26·0 and 28·6 keV are collected at the electrode at −20 kV. These results show energy sorting in the collector region with two depressed collectors for a case of small spread in energy, arising out of relatively low electronic efficiency.

For larger electronic efficiency, it would be necessary to include a more precise model of the energy spread in the beam arising out of the rf interaction. A larger number of depressed collectors would also be desirable for the case where electronic efficiency is high.

Furthermore, trajectory simulation for 14·5 keV shows a tendency for some electrons to be reflected before touching the −12·5 kV electrode. This indicates a residual rotational energy of 2 keV for some electrons. This phenomenon is minimized by suitable profiling of the magnetic and electrostatic fields. It also points up the benefit accruing from the transformation from rotational to axial motion, failing which, for example, the collection of the 23·4 keV electrons on the −20 kV electrode would not have been possible.

Since the value of the axial magnetic field is reduced as the beam proceeds farther into the collector region, a further conversion of the rotational motion into axial motion occurs. The reduction in magnetic field here need not be slow enough to qualify for being called adiabatic.

For comparison, it may be noted that if the reduction in α were to be obtained purely by adiabatic change of magnetic field, then

$$\alpha = [(\alpha_0^{-2} + 1)f_m - 1]^{-1/2} \tag{6}$$

where α_0 and α represent the ratio of transverse to axial velocity before and after the adiabatic change, and f_m is the ratio of initial to final value of the magnetic field. Correspondingly, the Larmor radius of the orbit increases by a factor of $\sqrt{f_m}$. For instance, starting with $\alpha_0 = 2$, an adiabatic reduction of magnetic field by a factor of nine would reduce α to 0·312 and increase the Larmor radius of the orbit by a factor of three.

These considerations can be used in designing any particular system, depending upon the nature of the device and the requirements as well as the space that could be made available in the radial and axial directions in the collector region.

4. Design considerations for the experiment

The computer simulation results described in the previous sections are used to provide guidelines for the design of the experiment. These guidelines are listed below. Recall that there are limitations in the modelling of the axial magnetic field at the beam radius by the function $\tanh z/\zeta$, especially as the particles travel to radii that are well-removed from the median radius of the beam.

1. As α is a function of starting radius, the range of variation of the latter is to be restricted (e.g. to 5%). Too large a spread in α_{midrange} would reduce the efficiency of rf interaction. Furthermore, if r_{start} has a narrow range, then the other parameters, such as B_0, V_0, and the location of the second cusp, can be fine tuned so that the α_{residual} is low for all the trajectories. However, as the range of r_{start} becomes narrower, the cathode current density for a given beam current would become higher; and thus become a limiting factor.

2. In order to minimize scalloping after passage through the first cusp, its transition width is to be minimized. The limiting factor would be the saturation flux of the material used. Presently ζ_1 is set at 4 mm, keeping the existing cusp number one as a starting point (Chojnacki *et al.* 1987).
3. The median values of other parameters are chosen so that the beam is scalloping inward as it enters the second cusp, minimizing α_{residual}.
4. The choice of the width of the second cusp is a design compromise. When the starting radius of the particles is restricted to a range less than 5% and the other parameters finely tuned, the minimum residual energy in the beam as a whole, associated with transverse motion beyond the second cusp, occurs when the two cusps are of comparable width. Increase of the width of the second cusp increases the residual energy by a few percentage points. However, this gives the advantage of an increased radial gap available for the beam to pass through. In this case, a cusp half width of 6 mm has been chosen.
5. The magnetic field profile, the electrode shapes, and their potentials are tailored to give optimum energy sorting between electrodes and soft landing of electrons with minimum residual energy.
6. The range of collection of electrons from 18·2–21 keV on the $-12{\cdot}5$ kV electrode and 22–28 keV on the -20 kV electrode is adequate for a device of electronic efficiency $\approx$10–15%. Such a typically low electronic efficiency for harmonic operation does not cause a large spread in the energies.

We are working toward an experimental confirmation of these ideas. We are also considering geometries involving larger numbers of depressed collectors.

5. Conclusions

The overall efficiency of devices employing spiralling electron beams can be raised appreciably by energy recovery from the spent beam. This can be done by 'unwinding' the beam before leading it to depressed collectors. A scheme for doing this has been proposed and analysed for the case of a large-orbit gyrotron. It involves the use of a second cusp with a reversed magnetic field for the purpose of beam-conditioning. It is seen that in this way a large fraction of the energy in the spent beam gets converted into energy of axial flow. Furthermore, the following conclusions emerge:

1. α_{residual} varies slowly with accelerating voltage.
2. α_{residual} varies cyclically with starting radius, magnetic field, and distance between cusps.
3. α_{residual} is a minimum when the scalloping motion of the electrons is inwards as they enter the second cusp.
4. The second cusp can be made wider than the first cusp to allow for a larger gap to let the spent electron beam through.
5. The combined action of the electrostatic field provided by depressed collectors of suitable shape and the magnetic field profile beyond the second cusp sorts the electron stream coming out of the latter onto the depressed collectors.

6. Collection at depressed potentials results in energy recovery. This enhancement of overall efficiency is feasible as well as particularly attractive for modes of operation that have low electronic efficiency.

The basic approach can be applied to other types of devices employing spiralling electron beams, for enhancing their overall efficiency.

Acknowledgments

The help rendered by Dr. E. P. Chojnacki is gratefully acknowledged. This work has been supported by the Air Force Office of Scientific Research.

References

Arnush, D., Boehmer, H., Caponi, M. Z., and Shih, C. C., 1982, Design of a high power CW free electron maser. *International Journal of Electronics*, **53,** 605–616.

Bekefi, G., Shefer, R. E., and Destler, W. W., 1986, Millimeter wave radiation from a rotating electron ring subjected to an azimuthally periodic wiggler magnetic field. *Nucl. Instrum. Methods Phys. Res.*, **A-250,** 352–356.

Chojnacki, E., Destler, W. W., Lawson, W., and Namkung, W., 1987, Studies of microwave radiation from a low-energy rotating electron beam in a multiresonator magnetron cavity. *Journal of Applied Physics*, **61,** 1268–1275.

Destler, W. W., and Rhee, M. J., 1977, Radial and axial compression of a hollow electron beam using an asymmetric magnetic cusp. *Physics of Fluids*, **20,** 1582–1584.

Destler, W. W., Chojnacki, E., Hoeberling, R. F., Lawson, W., Singh, A., and Striffler, C. D., 1988, High power microwave generation from large-orbit devices. To be published, *IEEE Trans. on Plasma Science*, April 1988.

Fix, A. Sh., *et al.*, 1984, The problems of increase in power, efficiency, and frequency of gyrotrons for plasma investigations. *International Journal of Electronics*, **57,** 821–826.

Granatstein, V. L., 1984, High average power and high peak power gyrotrons: present capabilities and future prospects. *International Journal of Electronics*, **57,** 787–799.

Granatstein, V. L., 1987, Status of high power gyrotron technology, *Proceedings of Particle Accelerator Conf.*, Washington DC, March (to be published).

Grow, R. W., and Shrivastava, U. A., 1982, Impedance calculations for travelling wave gyrotrons operating at harmonics of cyclotron frequency in magnetron type circuits operating in the π mode. *International Journal of Electronics*, **53,** 699–707.

Herrmannsfeldt, W. B., 1979, Electron trajectory program. SLAC Report 226, November.

Kosmahl, H. G., 1982, Modern multistage depressed collectors, A review. *Proc. IEEE*, **70,** 1325–1334.

Lau, Y. Y., and Barnett, L. R., 1982, Theory of a low magnetic field gyrotron (Gyromagnetron). *Int. J. Infrared Millimeter Waves*, **3,** 619–644.

Lawson, W., Destler, W. W., and Striffler, C. D., 1985, High-power microwave generation from a large-orbit gyrotron in vane and hole-and-slot conducting wall geometries. *IEEE Trans. Plasma Science*, **PS-13,** 444–453.

Lawson, W., and Latham, P. E., 1987, The design of a small-orbit/large-orbit gryroklystron experiment. *Journal of Applied Physics*, **61,** 519–528.

Rager, J. P., 1986, Gyrotron development in the framework of European fusion programme. *International Journal of Electronics*, **61,** 697–700.

Rhee, M. J., and Destler, W. W., 1974, Relativistic electron dynamics in a cusped magnetic field. *Physics of fluids*, **17,** 1574–1581.

Scheitrum, G. P., and True, R., 1981, A triple pole piece magnetic field reversal element for generation of high rotational energy beams. *Tech. Digest IEDM*, 332–334.

True, R., 1987, Emittance and the design of beam formation, transport and collection systems in periodically focussed TWT's. *IEEE Trans. Electron Devices*, **ED-34,** 473–485.

Uhm, H. S., Kim, C. M., and Namkung, W., 1984, Linear theory of cusptron microwave tube. *Physics of Fluids*, **27,** 488–498.